

Cumulene carbenes in TMC-1: Astronomical discovery of $l\text{-H}_2\text{C}_5$ [★]

C. Cabezas¹, B. Tercero^{2,3}, M. Agúndez¹, N. Marcelino¹, J. R. Pardo¹, P. de Vicente³ and J. Cernicharo¹

¹ Grupo de Astrofísica Molecular, Instituto de Física Fundamental (IFF-CSIC), C/ Serrano 121, 28006 Madrid, Spain. e-mail: carlos.cabezas@csic.es; jose.cernicharo@csic.es

² Observatorio Astronómico Nacional (IGN), C/ Alfonso XII, 3, 28014, Madrid, Spain.

³ Centro de Desarrollos Tecnológicos, Observatorio de Yebes (IGN), 19141 Yebes, Guadalajara, Spain.

Received; accepted

ABSTRACT

We report the first detection in space of the cumulene carbon chain $l\text{-H}_2\text{C}_5$. A total of eleven rotational transitions, with $J_{up} = 7\text{-}10$ and $K_a = 0$ and 1, were detected in TMC-1 in the 31.0-50.4 GHz range using the Yebes 40m radio telescope. We derive a column density of $(1.8 \pm 0.5) \times 10^{10} \text{ cm}^{-2}$. In addition, we report observations of other cumulene carbenes detected previously in TMC-1, to compare their abundances with the newly detected cumulene carbene chain. We find that $l\text{-H}_2\text{C}_5$ is ~ 4.0 times less abundant than the larger cumulene carbene $l\text{-H}_2\text{C}_6$, while it is ~ 300 and ~ 500 times less abundant than the shorter chains $l\text{-H}_2\text{C}_3$ and $l\text{-H}_2\text{C}_4$. We discuss the most likely gas-phase chemical routes to these cumulenes in TMC-1 and stress that chemical kinetics studies able to distinguish between different isomers are needed to shed light on the chemistry of C_nH_2 isomers with $n > 3$.

Key words. Astrochemistry — ISM: molecules — ISM: individual (TMC-1) — line: identification — molecular data

1. Introduction

Cumulene carbenes are highly polar carbon-chains with elemental formula H_2C_n . They contain consecutive carbon-carbon double bonds and two nonbonded electrons localized on the terminal C atom. These species play major roles as reaction intermediates in combustion and plasma processes and they are also of astrophysical interest since some of them have been detected in interstellar and circumstellar environments. The first astronomical discovery of the simplest cumulene carbene propadienyliene, $l\text{-H}_2\text{C}_3$, was carried out by Cernicharo et al. (1991a) toward the cold dark cloud TMC-1. Butatrienyliene, $l\text{-H}_2\text{C}_4$, was detected in the carbon-rich circumstellar envelope of IRC+10216 by Cernicharo et al. (1991b) and in TMC-1 by Kawaguchi et al. (1991) and later, the larger cumulene carbene hexapentaenyliene, $l\text{-H}_2\text{C}_6$, was detected in TMC-1, IRC+10216 and L1527 (Langer et al. 1997; Guélin et al. 2000; Araki et al. 2017).

Cumulene carbenes are metastable isomers, lying 0.5-0.6 eV above the most stable isomer, which is a polyacetylene (HC_nH) for an even n or a cyclic structure when the number of carbon atoms is odd. Thus, their astronomical detection demonstrates how far from thermochemical equilibrium is the composition of interstellar clouds. The case of HNC, which is less stable than HCN by about 0.6 eV but as abundant as HCN (Herbst 1978), illustrates this point as well.

Pentatetraenyliene, $l\text{-H}_2\text{C}_5$, is the cumulene carbene from the isomeric family with formula C_5H_2 . $l\text{-H}_2\text{C}_5$ is a high energy isomer and lies 0.564 eV above the most stable isomers, the nonpolar pentadienyliene (HCCCCH) and ethynyl cyclopropenyliene ($c\text{-C}_3\text{HCCH}$), whose energy separation is very small ~ 0.043 eV. Other two species are part of this isomeric fam-

ily, HCCCCH and $c\text{-C}_3\text{H}_2\text{C}_2$, placed at 0.737 and 0.910 eV above the most stable forms, respectively (Seburg et al. 1997). All these isomers, except the nonpolar HCCCCH, have been studied in the laboratory (Travers et al. 1997; McCarthy et al. 1997; Gottlieb et al. 1998) and, thus, their transition frequencies are well known. However, until very recently none of them has been observed in space. Cernicharo et al. (2021a) have reported the first identification in TMC-1 of the most stable isomer of this family, $c\text{-C}_3\text{HCCH}$, using a high sensitivity line survey gathered with the Yebes 40m radio telescope. This achievement opens the door to the identification of high energy isomers of this family in TMC-1.

In this Letter we report the first identification of the $l\text{-H}_2\text{C}_5$ cumulene carbene in space towards TMC-1 and a comparative study of the previously detected cumulene carbenes in this source. The derived column densities for these singular energetic species are interpreted by chemical models and used to understand the chemical processes leading to their formation.

2. Observations

The data presented in this work are part of a deep spectral line survey in the Q band towards TMC-1 ($\alpha_{J2000} = 4^{\text{h}}41^{\text{m}}41.9^{\text{s}}$ and $\delta_{J2000} = +25^{\circ}41'27.0''$) that was performed at the Yebes 40m radio telescope between November 2019 and April 2021. The survey was done using new receivers, built within the Nanocosmos project¹ consisting of two HEMT cold amplifiers covering the 31.0-50.4 GHz band with horizontal and vertical polarizations. Fast Fourier transform spectrometers (FFTSs) with 8×2.5 GHz bands per lineal polarization allow a simultaneous scan of a bandwidth of 18 GHz at a spectral resolution of 38.15 kHz. This setup has been described before by Tercero et al. (2021).

The observations were performed using the frequency switching technique with a frequency throw of 10 MHz or

¹ <https://nanocosmos.iff.csic.es/>

[★] Based on observations carried out with the Yebes 40m telescope (projects 19A003, 20A014, and 20D15). The 40m radiotelescope at Yebes Observatory is operated by the Spanish Geographic Institute (IGN, Ministerio de Transportes, Movilidad y Agenda Urbana).

8 MHz (see, e.g., Cernicharo et al. 2021b,c). The intensity scale, antenna temperature (T_A^*), for the two telescopes used in this work was calibrated using two absorbers at different temperatures and the atmospheric transmission model ATM (Cernicharo 1985; Pardo et al. 2001). Different frequency coverages were observed, 31.08–49.52 GHz and 31.98–50.42 GHz, which permitted us to check that no spurious ghosts are produced in the down-conversion chain. The signal coming from the receiver is down-converted to 1–19.5 GHz, and then split into 8 bands with a coverage of 2.5 GHz each of which are analyzed by the FFTs.

Pointing and focus corrections were obtained by observing strong SiO masers towards nearby evolved stars (IKTau and UOri). Pointing errors were always within $2'' - 3''$. Total calibration uncertainties have been adopted to be 10 % based on the observed repeatability of the line intensities between different observing runs. All data have been analyzed using the GILDAS package².

3. Results and discussion

3.1. Detection of l -H₂C₅ in TMC-1

l -H₂C₅ was observed in the laboratory by McCarthy et al. (1997) and the prediction of its rotational spectrum is available in the CDMS (Müller et al. 2005). This prediction, based in the laboratory data from McCarthy et al. (1997), is implemented in the MADEX code (Cernicharo 2012) that was used to identify the spectral features in our TMC-1 Q-band survey. McCarthy et al. (1997) observed in the laboratory a total of nine rotational transitions for l -H₂C₅ up to $J_{up}=5$ at 23 GHz. The derived parameters from McCarthy et al. (1997) (see Table 1) allow to accurately predict the rotational transitions for l -H₂C₅ in the Q-band. The molecule has a dipole moment of 5.9 D (Maluendes & McLean 1992) which makes it a very promising candidate to be observed in our TMC-1 data. In this manner, we search for this species in our TMC-1 survey and we found a total of eleven transitions ranging from $J_{up} = 7$ –10, whose frequencies agree very well with those predicted, discrepancies are smaller than 25 kHz. $9_{0,9} - 8_{0,8}$ line is blended with a negative feature produced in the folding of the frequency switching data while $10_{0,10} - 9_{0,9}$ transition is not detected due to the limited sensitivity at the predicted frequency. In any case the non-detection is consistent with the expected intensity. All the l -H₂C₅ lines observed in TMC-1, shown in Fig. 1 and listed in Table 2, were analyzed, together with those observed in laboratory, using an asymmetric rotor Hamiltonian with the FITWAT code (Cernicharo et al. 2018) to derive the rotational and centrifugal distortion constants. The results from this fit are shown in Table 1 together with those obtained by McCarthy et al. (1997) only with laboratory data. With this new global fit an improvement of the uncertainty in the rotational and distortion constants is obtained. Hence, this fit is recommended to predict the frequency of the rotational transitions of l -H₂C₅ with uncertainties between 10 and 200 kHz in the 50–116 GHz frequency range.

As l -H₂C₅ has C_{2v} symmetry, it is necessary to discern between ortho- l -H₂C₅ and para- l -H₂C₅. The ortho levels are described by K_a odd while the para levels by K_a even. The nuclear spin-weights are 3 and 1 for ortho- l -H₂C₅ and para- l -H₂C₅, respectively. The $J_{K_a, K_c} = 1_{1,1}$ is the lowest ortho energy state located 13.4 K above the para ground level, $J_{K_a, K_c} = 0_{0,0}$. Hence, from the eleven observed lines eight of them correspond to ortho- l -H₂C₅ and the remain-

Table 1. New derived rotational parameters (in MHz) for l -H₂C₅.

Constant	TMC-1+Lab ^a	Lab ^b
A	277600.0 ^c	277600.0
B	2304.78432(27)	2304.7844(3)
C	2285.80518(27)	2285.8053(3)
$\Delta_J \times 10^3$	0.0978(19)	0.104(6)
Δ_{JK}	0.04647(19)	0.0464(2)
rms^d	8.7	3.0
J_{min}/J_{max}	2/10	2/5
K_{min}/K_{max}	0/1	0/1
N^e	20	9

Notes. ^(a) Fit to the lines of l -H₂C₅ observed in TMC-1 and in laboratory (McCarthy et al. 1997). ^(b) (McCarthy et al. 1997). ^(c) Fixed to the value reported by McCarthy et al. (1997). ^(d) The standard deviation of the fit in kHz. ^(e) Number of lines included in the fit.

ing three to para- l -H₂C₅. An analysis of the line intensities through a line model fitting procedure Cernicharo et al. (2021a) provides a rotational temperature of ~ 10 K and column densities $N(\text{ortho-}l\text{-H}_2\text{C}_5) = (1.3 \pm 0.3) \times 10^{10} \text{ cm}^{-2}$ and $N(\text{para-}l\text{-H}_2\text{C}_5) = (5.0 \pm 2.0) \times 10^9 \text{ cm}^{-2}$. The ortho/para ratio is calculated to be 2.6 ± 1.5 . We have assumed a linewidth of 0.6 km s^{-1} and a source of uniform brightness temperature with a diameter of $80''$ (Fossé et al. 2001). Figure 1 shows, in red, the computed synthetic spectrum.

3.2. Column densities for l -H₂C₃, l -H₂C₄ and l -H₂C₆ in TMC-1

The carbene l -H₂C₃ is the smallest cumulene species studied in this work. The laboratory spectroscopic data used to predict the l -H₂C₃ spectrum were reported by Vrtilek et al. (1990). The electric dipole moment calculated for this molecule is 4.1 D (Defrees & McLean 1986). As for l -H₂C₅, l -H₂C₃ has C_{2v} symmetry and, thus, it is necessary to discern between ortho and para l -H₂C₃. In the same manner than for l -H₂C₅ the ortho levels are described by K_a odd while the para levels by K_a even, with 3/1 ratio for ortho/para. Only three rotational transitions for l -H₂C₃ lie within the 31.0–50.4 GHz frequency range. One transition, $2_{0,2} - 1_{0,1}$, corresponds to para- l -H₂C₃ and the other two, $2_{1,2} - 1_{1,1}$ and $2_{1,1} - 1_{1,0}$ are ortho- l -H₂C₃ transitions. The lines are shown in Fig. 2 while the line parameters are collected in Table 2. The position of the lines is consistent with the calculated frequencies and the systemic velocity of the source, $V_{LSR} = 5.83 \text{ km s}^{-1}$ (Cernicharo et al. 2020). We assumed $T_r = 10$ K and the column densities $N(\text{ortho-}l\text{-H}_2\text{C}_3) = (1.5 \pm 0.5) \times 10^{12} \text{ cm}^{-2}$ and $N(\text{para-}l\text{-H}_2\text{C}_3) = (4.0 \pm 1.2) \times 10^{11} \text{ cm}^{-2}$. The ortho/para ratio is calculated to be 3.8 ± 1.1 . Collisional rates are available for the system l -H₂C₃/He (Khalifa et al. 2019). Adopting a volume density for TMC-1 of $4 \times 10^4 \text{ cm}^{-3}$ (Cernicharo & Guélin 1987; Fossé et al. 2001) we derive an excitation temperature for the two ortho transitions of ~ 9 K, and of ~ 8.5 K for the para transition. Hence, the adopted rotational temperature seems well adapted to the excitation conditions of this molecule.

The next member of the l -H₂C_{*n*} family is l -H₂C₄. The rotational spectrum for this cumulene was observed by Killian et al. (1990) and Travers et al. (1996). From ab initio calculations the dipole moment of l -H₂C₄ has been estimated to be 4.1 D (Oswald & Botschwina 1995), similar to the smaller cumulene carbene l -H₂C₃. The lines for ortho- and para- l -H₂C₄ are clearly detected in our TMC-1 survey as can be seen in Fig. 3. However, it should be noted that there are small discrepancies (of about 30 kHz for the para species) between the observed and predicted

² <http://www.iram.fr/IRAMFR/GILDAS>

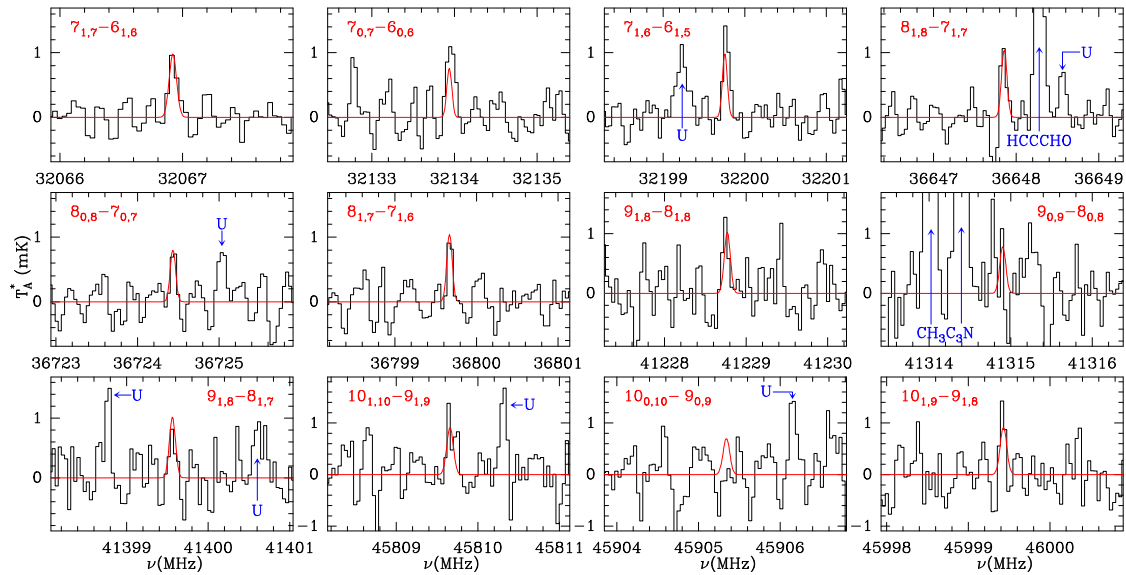


Fig. 1. Observed lines of $l\text{-H}_2\text{C}_5$ in TMC-1 in the 31.0-50.4 GHz range. The abscissa corresponds to the rest frequency assuming a local standard of rest velocity of 5.83 km s^{-1} . The ordinate is antenna temperature in millikelvins. Curves shown in red are the computed synthetic spectra. U labels correspond to features above 4σ . Frequencies and line parameters are given in Table 2.

Table 2. Observed lines of $l\text{-H}_2\text{C}_3$, $l\text{-H}_2\text{C}_4$, $l\text{-H}_2\text{C}_5$, and $l\text{-H}_2\text{C}_6$ towards TMC-1.

State	Transition ($J_{K_a, K_c})_u - (J_{K_a, K_c})_l$	Rest Freq. (MHz)	E_{up} (K)	S_{ij}	$\int T_A^* dv$ (mK km s $^{-1}$)	V_{LSR} (km s $^{-1}$)	Δv (km s $^{-1}$)	T_A^* (mK)
<i>l</i> -H ₂ C ₃								
<i>ortho</i>	2 _{1,2} – 1 _{1,1}	41198.335(2)	2.0	1.50	72.0208(2)	5.71(1)	0.61(1)	110.3(3)
<i>para</i>	2 _{0,2} – 1 _{0,1}	41584.675(1)	3.0	2.00	50.0199(4)	5.75(1)	0.58(1)	81.11(3)
<i>ortho</i>	2 _{1,1} – 1 _{1,0}	41967.671(2)	2.0	1.50	72.2521(2)	5.75(1)	0.56(1)	122.5(3)
<i>l</i> -H ₂ C ₄								
<i>ortho</i>	4 _{1,4} – 3 _{1,3}	35577.008(2)	3.8	3.75	137.590(1)	5.71(1)	0.70(1)	185.3(2)
<i>para</i>	4 _{0,4} – 3 _{0,3}	35727.379(1)	4.3	4.00	91.6939(2)	5.53(1)	0.67(1)	128.0(2)
<i>ortho</i>	4 _{1,3} – 3 _{1,2}	35875.775(2)	3.9	3.75	140.130(1)	5.69(1)	0.69(1)	189.9(2)
<i>ortho</i>	5 _{1,5} – 4 _{1,4}	44471.137(2)	6.0	4.80	120.160(1)	5.72(1)	0.57(1)	199.4(4)
<i>para</i>	5 _{0,5} – 4 _{0,4}	44659.015(1)	6.0	5.00	73.0765(2)	5.58(1)	0.58(1)	119.2(4)
<i>ortho</i>	5 _{1,4} – 4 _{1,3}	44844.590(2)	6.4	4.80	117.010(1)	5.70(1)	0.59(1)	186.6(4)
<i>l</i> -H ₂ C ₅								
<i>ortho</i>	7 _{1,7} – 6 _{1,6}	32066.902(2)	5.9	6.86	0.6759(5)	5.83(7)	0.69(17)	0.9(2)
<i>para</i>	7 _{0,7} – 6 _{0,6}	32133.937(2)	6.2	7.00	1.3465(2)	5.83(8)	1.06(16)	1.2(2)
<i>ortho</i>	7 _{1,6} – 6 _{1,5}	32199.756(2)	6.0	6.86	1.1423(2)	5.83(5)	0.77(12)	1.4(2)
<i>ortho</i>	8 _{1,8} – 7 _{1,7}	36647.836(3)	7.7	7.88	0.7123(5)	5.71(8)	0.58(13)	1.2(3)
<i>para</i>	8 _{0,8} – 7 _{0,7}	36724.433(3)	7.9	8.00	0.5152(11)	5.83(8)	0.53(23)	0.9(3)
<i>ortho</i>	8 _{1,7} – 7 _{1,6}	36799.669(3)	7.7	7.88	0.5908(7)	5.83(5)	0.48(19)	1.2(2)
<i>ortho</i>	9 _{1,9} – 8 _{1,8}	41228.749(4)	9.7	8.89	0.7447(6)	5.83(8)	0.54(16)	1.2(4)
<i>para</i>	9 _{0,9} – 8 _{0,8}	41314.902(5)	9.9	9.00	^(a)
<i>ortho</i>	9 _{1,8} – 8 _{1,7}	41399.562(4)	9.7	8.89	0.4890(14)	5.83(9)	0.59(29)	0.8(4)
<i>ortho</i>	10 _{1,10} – 9 _{1,9}	45809.639(6)	11.9	9.90	0.5462(8)	5.83(7)	0.37(11)	1.4(4)
<i>para</i>	10 _{0,10} – 9 _{0,9}	45905.342(7)	12.1	10.0	^(b)
<i>ortho</i>	10 _{1,9} – 9 _{1,8}	45999.431(6)	11.9	9.90	0.6841(5)	5.83(7)	0.42(10)	1.5(4)
<i>l</i> -H ₂ C ₆								
<i>ortho</i>	12 _{1,12} – 11 _{1,11}	32232.270(6)	9.9	11.9	3.89347(2)	5.82(2)	0.80(5)	4.6(2)
<i>para</i>	12 _{0,12} – 11 _{0,11}	32273.061(6)	10.1	12.0	2.25233(5)	5.86(3)	0.73(7)	2.9(2)
<i>ortho</i>	12 _{1,11} – 11 _{1,10}	32313.117(6)	10.0	11.9	4.17934(2)	5.83(2)	0.81(5)	4.8(3)
<i>ortho</i>	13 _{1,13} – 12 _{1,12}	34918.254(8)	11.6	12.9	3.58530(2)	5.84(2)	0.66(4)	5.1(3)
<i>para</i>	13 _{0,13} – 12 _{0,12}	34962.439(8)	11.7	13.0	2.61780(6)	5.86(4)	0.91(9)	2.7(3)
<i>ortho</i>	13 _{1,12} – 12 _{1,11}	35005.838(8)	11.6	12.9	3.52717(2)	5.83(1)	0.70(4)	4.7(2)
<i>ortho</i>	14 _{1,14} – 13 _{1,13}	37604.22(1)	13.4	13.9	2.95633(3)	5.80(2)	0.67(4)	4.1(2)
<i>para</i>	14 _{0,14} – 13 _{0,13}	37651.80(1)	13.6	14.0	1.73602(10)	5.83(4)	0.70(9)	2.3(3)
<i>ortho</i>	14 _{1,13} – 13 _{1,12}	37698.54(1)	13.4	13.9	2.87938(3)	5.80(2)	0.73(5)	3.7(2)
<i>ortho</i>	15 _{1,15} – 14 _{1,14}	40290.19(1)	15.3	14.9	2.58873(5)	5.75(2)	0.56(5)	4.4(4)
<i>para</i>	15 _{0,15} – 14 _{0,14}	40341.16(1)	15.5	15.0	1.95729(10)	5.87(5)	0.76(9)	2.4(4)
<i>ortho</i>	15 _{1,14} – 14 _{1,13}	40391.25(1)	15.4	14.9	2.47566(5)	5.91(3)	0.65(8)	3.6(2)
<i>ortho</i>	16 _{1,16} – 15 _{1,15}	42976.15(2)	17.4	15.9	1.2139(2)	5.92(4)	0.48(7)	2.4(3)
<i>para</i>	16 _{0,16} – 15 _{0,15}	43030.51(2)	17.6	16.0	0.7463(4)	5.80(6)	0.50(12)	1.4(3)
<i>ortho</i>	16 _{1,15} – 15 _{1,14}	43083.94(2)	17.4	15.9	1.61939(11)	5.88(3)	0.62(8)	2.5(3)
<i>ortho</i>	17 _{1,17} – 16 _{1,16}	45662.09(2)	19.6	16.9	1.0792(4)	5.86(9)	0.68(23)	1.5(5)
<i>para</i>	17 _{0,17} – 16 _{0,16}	45719.84(2)	19.7	17.0	1.3389(2)	5.92(6)	0.61(12)	2.1(4)
<i>ortho</i>	17 _{1,16} – 16 _{1,15}	45776.62(2)	19.6	16.9	0.6063(12)	5.85(9)	0.45(24)	1.3(6)
<i>ortho</i>	18 _{1,18} – 17 _{1,17}	48348.02(2)	21.9	17.9	1.3459(3)	5.72(9)	0.68(19)	1.8(6)
<i>para</i>	18 _{0,18} – 17 _{0,17}	48409.16(2)	22.1	18.0	0.36152(11)	5.82(9)	0.23(90)	1.4(6)
<i>ortho</i>	18 _{1,17} – 17 _{1,16}	48469.29(2)	22.0	17.9	0.37677(10)	6.27(5)	0.23(90)	1.5(6)

Notes. Numbers in parentheses indicate the uncertainty in units of the last significant digits. For the observational parameters we adopted the uncertainty of the Gaussian fit provided by GILDAS. ^(a) One-channel spectral feature. ^(b) Spectral feature below the noise level.

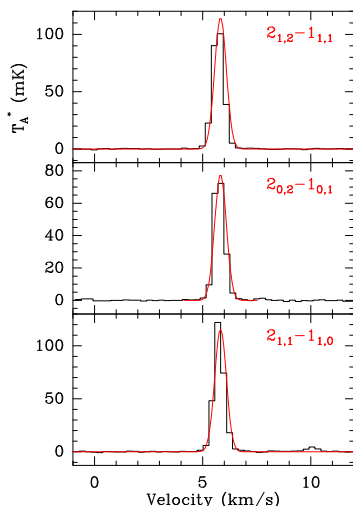


Fig. 2. Observed lines of l -H₂C₃ in TMC-1 in the 31.0-50.4 GHz range. Curves shown in red are the computed synthetic spectra. Frequencies and line parameters are given in Table 2.

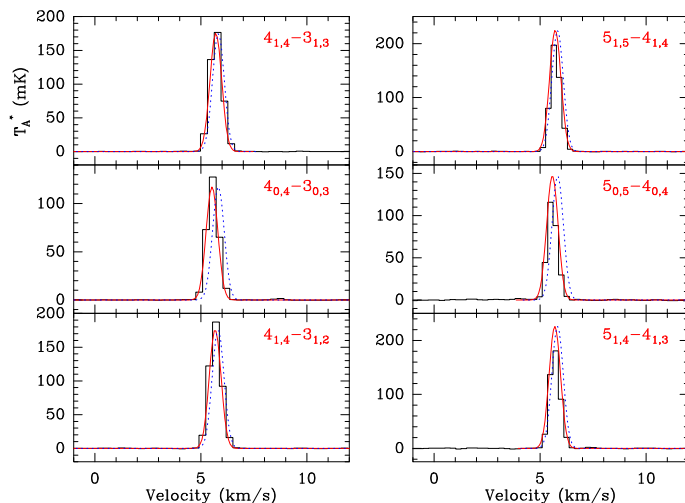


Fig. 3. Observed lines of l -H₂C₄ in TMC-1 in the 31.0-50.4 GHz range. Curves shown in red and green are the computed synthetic spectra using the observed frequencies and the CDMS predictions, respectively. Frequencies and line parameters are given in Table 2.

frequencies from CDMS. We observed a total of six rotational transitions with $J_{up} = 4$ and 5 and $K_a = 0$ and 1. Four of them pertain to ortho- l -H₂C₄ and two to para- l -H₂C₄. All the line parameters are given in Table 2. From the observed integrated line intensities we obtained a $T_r = 10$ K and column densities for the ortho and para species of $N(\text{ortho-}l\text{-H}_2\text{C}_4) = (2.5 \pm 0.8) \times 10^{12} \text{ cm}^{-2}$ and $N(\text{para-}l\text{-H}_2\text{C}_4) = (8.0 \pm 2.3) \times 10^{11} \text{ cm}^{-2}$. The ortho/para ratio for l -H₂C₄ is 3.1 ± 0.9 .

l -H₂C₆ is, to date, the larger cumulene carbene observed in space. Its dipole moment is calculated (Maluendes & McLean 1992) to be larger than those for the smaller cumulenes, with a value of 6.2 D. The rotational spectrum has been investigated by McCarthy et al. (1997) and the derived spectroscopic parameters are used to predict its transition frequencies. Due to its larger molecular size, many rotational transition for l -H₂C₆ can be observed in the 31.0-50.4 GHz frequency range. As for all the other cumulene carbenes, and due to its symmetry, it is necessary to discern between ortho- and para- l -H₂C₆. Hence, we observed a total of twenty-one transitions for l -H₂C₆, four-

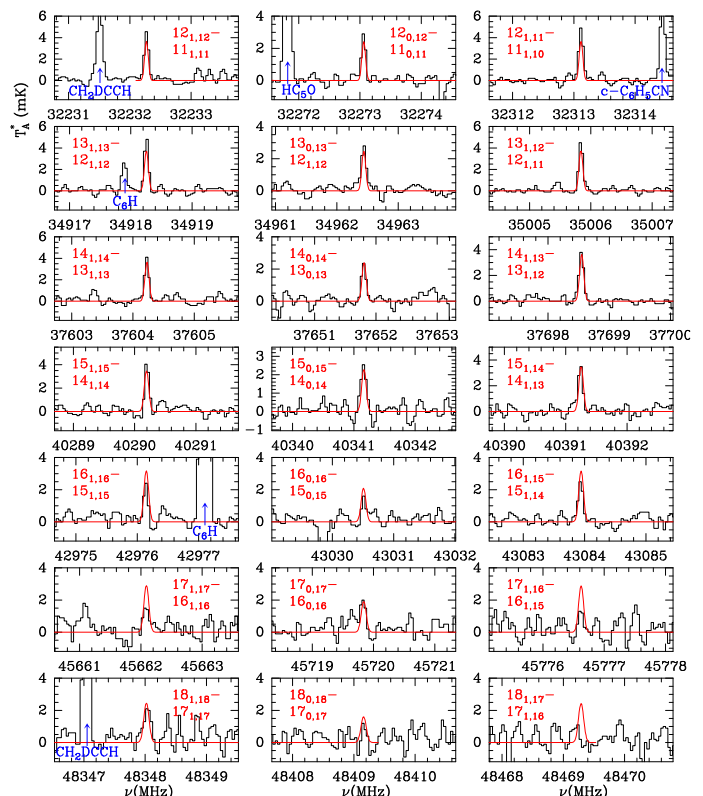


Fig. 4. Observed lines of l -H₂C₆ in TMC-1 in the 31.0-50.4 GHz range. Curves shown in red are the computed synthetic spectra. Frequencies and line parameters are given in Table 2.

teen for ortho- and seven for para- l -H₂C₆ (see Fig. 4). Line parameters are collected in Table 2. We derived from the observed integrated line intensities a $T_r = 10$ K and the column densities $N(\text{ortho-}l\text{-H}_2\text{C}_6) = (6.0 \pm 1.8) \times 10^{10} \text{ cm}^{-2}$ and $N(\text{para-}l\text{-H}_2\text{C}_6) = (2.0 \pm 0.6) \times 10^{10} \text{ cm}^{-2}$. The ortho/para ratio is calculated to be 3.0 ± 0.9 .

From our observations we obtain the following relative abundances for l -H₂C₃/ l -H₂C₄/ l -H₂C₅/ l -H₂C₆ in TMC-1, 344/561/1/4.4. l -H₂C₄ is the most abundant cumulene carbene in TMC-1, followed by l -H₂C₃. The larger species l -H₂C₅ and l -H₂C₆ are much less abundant compared to the shorter cumulene chain, with l -H₂C₆ being 4.4 times more abundant than the odd member l -H₂C₅. It is worth noting that, within the uncertainties, the four cumulenes studied in this work have an ortho/para abundance ratio of 3. Hence, no significant ortho to para conversion can be noticed for these molecules.

3.3. Chemistry of cumulene carbenes

In order to understand how cumulene carbenes l -H₂C _{n} can be formed in TMC-1, we carried out gas-phase chemical modeling calculations. We adopted typical conditions of cold dark clouds, i.e., a volume density of H nuclei of $2 \times 10^4 \text{ cm}^{-3}$, a gas kinetic temperature of 10 K, a visual extinction of 30 mag, a cosmic-ray ionization rate of H₂ of $1.3 \times 10^{-17} \text{ s}^{-1}$, and the so-called set of low-metal elemental abundances (e.g., Agúndez & Wakelam 2013). We used the chemical network RATE12 from the UMIST database (McElroy et al. 2013), updated with results from Lin et al. (2013), and expanded with the subset of gas-phase chemical reactions revised by Loison et al. (2017) in their study of the chemistry of C₃H and C₃H₂ isomers.

Among the family of carbenes $l\text{-H}_2\text{C}_n$, the one for which the chemistry is better constrained is by far the smallest member $l\text{-H}_2\text{C}_3$, which has been discussed in detail by Loison et al. (2017). This species is mainly formed upon dissociative recombination with electrons of the linear and cyclic isomers of C_3H_3^+ , which in turn are formed through the radiative association of C_3H^+ and H_2 . If we focus in the so-called early time, a few 10^5 yr, where gas-phase chemical models of cold dark clouds reproduce better TMC-1 observations (e.g., Agúndez & Wakelam 2013), the calculated abundance is about one order of magnitude below the observed value (see Fig. 5), but the calculated cyclic-to-linear abundance ratio agrees very well with the observed value of 31 (Cernicharo et al. 2021a; this work). For members of the series $l\text{-H}_2\text{C}_n$ with $n > 3$, information on the chemistry of the different possible isomers is poorly known and thus chemical networks, such as UMIST RATE12, do not distinguish between them. The calculated abundances of C_4H_2 and C_6H_2 agree within a factor of 2-3 with the observed abundances of $l\text{-H}_2\text{C}_4$ and $l\text{-H}_2\text{C}_6$, respectively (see Fig. 5), although one must keep in mind that observations only refer to the cumulene while the model includes also other isomers, in particular the more stable non-polar species HC_nH . If the isomer HC_nH is significantly more abundant than H_2C_n for $n = 4, 6$ in TMC-1, then the abundances calculated by the chemical model for C_4H_2 and C_6H_2 would be too low. In the case of C_5H_2 , the calculated peak abundance is about 30 times lower than the observed abundance of $l\text{-H}_2\text{C}_5$ (see Fig. 5), although this may not be a problem if the more stable isomer HC_5H is substantially more abundant than the carbene $l\text{-H}_2\text{C}_5$.

For $l\text{-H}_2\text{C}_n$ with $n > 3$, the chemical route analogous to that forming $l\text{-H}_2\text{C}_3$ has variable degrees of efficiency. For example, formation of C_4H_3^+ is relatively efficient thanks to the radiative association between C_4H_2^+ and H (McEwan et al. 1999). For $n = 5$, the route does not work because C_5H^+ does not react with H_2 (McElvany et al. 1987; Bohme & Wlodek 1990), while formation of C_6H_3^+ is uncertain due to the unknown reactivity of C_6H_2^+ with H_2 (Anicich 2003). Further studies of reactions involving hydrocarbon ions, in particular regarding isomer differentiation, are highly desirable. According to the chemical model, reactions of C_nH^- anions with H atoms are a major route to C_nH_2 molecules, such as C_4H_2 , C_5H_2 , and C_6H_2 . These reactions have been studied in the laboratory for anions C_nH^- with $n = 2, 4, 6$, and 7 and have been found to be rapid and to yield C_nH_2 as main product (Barckholtz et al. 2001). The reaction with $n = 5$, although not studied, is likely to behave similarly. It is however unknown whether the carbene isomer H_2C_n or the more stable HC_nH is preferentially formed. It would be very helpful to investigate this particular point.

Other formation routes, apart from $\text{C}_n\text{H}_m^+ + e^-$ and $\text{C}_n\text{H}^- + \text{H}$, can be provided by neutral-neutral reactions. For example, the chemical model points to the reaction between atomic C and the propargyl radical (CH_2CCH), recently detected in TMC-1 (Agúndez et al. 2021), as a source of C_4H_2 isomers. This reaction is assumed to be fast by Loison et al. (2017), but calculations of the rate coefficient and product distribution at low temperatures are needed. Similarly, the reaction $\text{C} + \text{C}_4\text{H}_3$ is assumed to proceed fast by Smith et al. (2004) and provides an important route to C_5H_2 isomers, but more detailed studies on this reaction are necessary. Finally, we note that the cyclic C_5H_2 isomer $c\text{-C}_3\text{HCCH}$ recently detected by Cernicharo et al. (2021a) is most likely formed through the reaction between CCH and $c\text{-C}_3\text{H}_2$.

Acknowledgements. This research has been funded by ERC through grant ERC-2013-Syg-610256-NANOCOSMOS. Authors also thank Ministerio de Ciencia e Innovación for funding support through projects AYA2016-75066-C2-1-P, PID2019-106235GB-I00 and PID2019-107115GB-C21 / AEI /

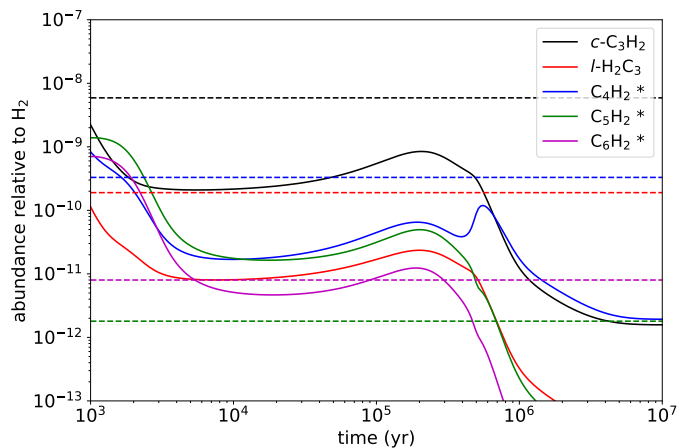


Fig. 5. Calculated fractional abundances of various hydrocarbons as a function of time. The symbol * in the legend means that the chemical model does not distinguish between different isomers. The abundances observed in TMC-1 for $c\text{-C}_3\text{H}_2$ (Cernicharo et al. 2021a) and $l\text{-H}_2\text{C}_n$ with $n = 3-6$ (this work) are indicated by dashed horizontal lines.

10.13039/501100011033. MA thanks Ministerio de Ciencia e Innovación for grant RyC-2014-16277.

References

- Agúndez, M., & Wakelam, V. 2013, *Chem. Rev.*, 113, 8710
 Agúndez, M., Cabezas, C., Tercero, B., et al. 2021, *A&A*, 647, L10
 Anicich, V. G. 2003, JPL Publication 03-19
 Araki, M., Takano, S., Sakai, N., et al. 2017, *ApJ*, 847, 51
 Barckholtz, C., Snow, T. P., & Bierbaum, V. M. 2001, *ApJ*, 547, L171
 Bohme, D. K. & Wlodek, S. 1990, *Int. J. Mass Spectrom. Ion Proc.*, 102, 133
 Cernicharo, J. 1985, Internal IRAM report (Granada: IRAM)
 Cernicharo, J. & Guélin, M. 1987, *A&A*, 176, 299
 Cernicharo, J., Gottlieb, C. A., Guélin, M., et al. 1991a, *ApJ*, 368, L39
 Cernicharo, J., Gottlieb, C. A., Guélin, M., et al. 1991b, *ApJ*, 368, L43
 Cernicharo, J., Heras, A.M., Tielens, A.G.G.M., et al., 2001, *ApJ*, 546, L123
 Cernicharo, J. 2012, in *European Conference on Laboratory Astrophysics*, eds. C. Stehlé, C. Joblin, & L. d'Hendecourt, *EAS Publication Series*, 58, 251
 Cernicharo, J., Guélin, M., Agúndez, M., et al. 2018, *A&A*, 618, A4
 Cernicharo, J., Marcelino, N., Agúndez, M., et al. 2020, *A&A*, 642, L8
 Cernicharo, J., Agúndez, M., Cabezas, C., et al. 2021a, *A&A*, in press
 Cernicharo, J., Cabezas, C., Endo, Y., et al. 2021b, *A&A*, 646, L3
 Cernicharo, J., Cabezas, C., Baillieux, S., et al. 2021c, *A&A*, 646, L7
 Defrees, D. J., & McLean, A. D., 1986, *ApJ*, 308, 31
 Fossé, D., Cernicharo, J., Gerin, M., Cox, P. 2001, *ApJ*, 552, 168
 Gottlieb, C.A., McCarthy, M.C., Gordon, V.D., et al. 1998, *ApJ*, 509, L141
 Guélin, M., Müller, S., Cernicharo, 2000, *A&A*, 363, L9
 Herbst, E., 1978, *ApJ*, 222, 508
 Kawaguchi, K., Kaifu, N., Ohishi, M., et al., 1991, *PASJ*, 43, 607
 Khalifa, M.B., Sahnoun, E., Wiesenfeld, L., et al. 2019, *Phys. Chem. Chem. Phys.*, 21, 1443
 Killian, T. C., Vrtilik, J. M., Gottlieb, C. A., et al., 1990, *ApJ*, 365, L89
 Langer, W. D., Velusamy, T., Kuiper, T. B. H., et al. 1997, *ApJ*, 480, L63
 Lin, Z., Talbi, D., Roueff, E., et al. 2013, *ApJ*, 765, 80
 Loison, J.-C., Agúndez, M., Wakelam, V., et al. 2017, *MNRAS*, 470, 4075
 Maluendes, S. A., & McLean, A. D. 1992, *Chem. Phys. Lett.*, 200, 511
 McCarthy, M.C., Travers, M.J.; Kovács, A., et al. 1997, *Science*, 275, 518
 McElroy, D., Walsh, C., Markwick, A. J., et al. 2013, *A&A*, 550, A36
 McElvany, S. W., Dunlap, B. I., & OKeefe, A. 1987, *J. Chem. Phys.*, 86, 715
 McEwan, M. J., Scott, G. B. I., Adams, N. G., et al. 1999, *ApJ*, 513, 287
 Müller, H. S. P., Schlöder, F., Stutzki, J., & Winnewisser, G. 2005, *J. Mol. Struct.*, 742, 215
 Oswald, M., & Botschwina, P., 1995, *J. Mol. Spectrosc.*, 169, 181.
 Pardo, J. R., Cernicharo, J., Serabyn, E. 2001, *IEEE Trans. Antennas and Propagation*, 49, 12
 Sattelmeyer, K. W., & Stanton, J. F., 2000, *J. Am. Chem. Soc.*, 122, 8220
 Seburg, R. A., McMahon, R. J., Stanton, J. F., & Gauss, J. 1997, *J. Am. Chem. Soc.*, 119, 10838
 Smith, I. W. M., Herbst, E., & Chang, Q. 2004, *MNRAS*, 350, 323
 Thaddeus, P., Vrtilik, J. M., & Gottlieb, C. A., 1985, *ApJ*, 299, L63
 Travers, M.J., Chen, W., Novick, S.E., et al. 1996, *J. Mol. Spectrosc.*, 180, 75
 Tercero, F., López-Pérez, J. A., Gallego, et al., 2021, *A&A*, 645, A37
 Travers, M.J., McCarthy, M.C., Gottlieb, C.A., & Thaddeus, P. 1997, *ApJ*, 483, L135
 Vrtilik, J. M., Gottlieb, C. A., Gottlieb, E. W., et al. 1990, *ApJ*, 364, L53